3D-printing of solid lipid tablets from emulsion gels

Jenny Johannesson [a,1], Jamal Khan [a,1], Madlen Hubert [a], Alexandra Teleki [b], Christel A. S. Bergström [a,*]

[a] Department of Pharmacy, Uppsala University, Uppsala Biomedical Center, P.O Box 580, SE-751 23 Uppsala, Sweden
[b] Department of Pharmacy, Science for Life Laboratory, Uppsala University, SE-751 23 Uppsala, Sweden

ARTICLE INFO

ABSTRACT

Interest in 3D-printing technologies for pharmaceutical manufacturing of oral dosage forms is driven by the need for personalized medicines. Most research to date has focused on printing of polymeric-based drug delivery systems at high temperatures. Furthermore, oral formulation development is continuously challenged by the large number of poorly water-soluble drugs, which require more advanced enabling formulations to improve oral bioavailability. In this work, we used semi-solid extrusion (SSE) printing of emulsion gels with three types of emulsified lipid-based formulations (LBFs) to produce solid lipid tablets incorporating the poorly water-soluble drug, fenofibrate. Tablets were successfully 3D-printed from emulsion gels using SSE at room temperature, making the methodology particularly useful for thermolabile compounds. The tablets were well-defined in mass and disintegrated rapidly (<15 min). Importantly, the oil droplet size reconstituted after dispersion of the tablets and subsequent lipid digestion was similar to traditional liquid LBFs. This work demonstrates the successful use of SSE for fabricating solid lipid tablets based on emulsion gels. The method is further promising for on demand production of personalized dosage forms, necessary for flexible dosage adjustment in e.g., pediatric patients, when poorly water-soluble compounds constitute the core of the therapy.

1. Introduction

Recently, 3D-printing technologies have revolutionized pharmaceutical manufacturing and paved the way for the development of personalized drug products (Awad et al., 2018; Norman et al., 2017). Interest in 3D-printing skyrocketed in 2015 after the US Food and Drug Administration (FDA) approved the first 3D-printed drug Spritam (levetiracetam), a highly porous tablet that disintegrates rapidly in the mouth. Traditional solid dosage forms, manufactured on large scale such as tablets, are simple and uniform. Such tablets are produced on a one size fits all assumption and typically demand manipulation e.g., splitting, crushing, and dispersing fragments of a tablet prior to administration to children (Bjerknes et al., 2017; van der Vossen et al., 2019). In contrast, 3D-printing technologies enable production of patient-tailored and flexible dosage forms, by easily adjusting dose, shape, and size of tablets on demand (i.e., in hospital pharmacies). These attributes align with the vision of the pharmaceutical industry to create personalized dosage forms. This personalization of medicines can benefit pediatric and geriatric patients in particular, as physiological differences are pronounced in these age groups and compliance to medication is low (El Aita et al., 2020; Öblom et al., 2019; Trenfield et al., 2018).

Only a few types of 3D-printing technologies have been explored for pharmaceutical manufacturing. The most studied is fused deposition modeling (FDM), an extrusion-based 3D-printing technique, in which polymeric filaments are melted, extruded through a nozzle, and then resolidified upon contact with the cool print bed. Complex dosage forms can be produced with FDM printing using different types of filaments in the same product, however, high temperatures are required and printing speed is slow (Norman et al., 2017; Okwuosa et al., 2017). Another type of extrusion-based 3D-printing technique, semi-solid extrusion (SSE), is designed for printing gels and pastes that exhibit appropriate rheological properties. The advantages of SSE are that it enables rapid printing at low temperature (Firth et al., 2018). From a pharmaceutical perspective, the latter attribute is of great importance for thermolabile drugs and heat-sensitive components of the formulation. SSE allows 3D-printing of personalized dosage forms with high drug loading and multiple drug

---

release profiles from different printed compartments (Khaled et al., 2018, Khaled et al., 2015a, 2015b). Moreover, the first application of SSE in a clinical setting was recently demonstrated by Goyanes and colleagues (Goyanes et al., 2019). Using 3D-printing, they produced personalized chewable dosage forms for the treatment of pediatric patients with a rare metabolic disease.

Most research on 3D-printed dosage forms has focused on water-soluble drugs without the demand for advanced formulation strategies to enable oral drug absorption. Incorporation of poorly water-soluble drugs into 3D-printed medicines has not been explored in detail, despite the large number of such drug candidates in pharmaceutical discovery (Bergström et al., 2016; Boyd et al., 2019). Lipophilic drugs have poor solubility in gastrointestinal fluids, so their oral administration typically relies on enabling formulations to improve bioavailability. A well-established enabling formulation is the use of lipid-based formulations (LBFs). Typically, the drug is predissolved in the liquid formulation, which is filled into gelatin capsules for oral administration. In recent years, LBFs that are mixtures of oils and surfactants, have gained increased interests as a means to increase absorption of poorly water-soluble drugs. These self-emulsifying drug delivery systems spontaneously form emulsion droplets in contact with aqueous media (Pouton, 1997; Rani et al., 2019). However, stability and manufacturing challenges associated with liquid LBFs hinder their commercial development and transformation of liquid LBFs into solid dosage forms would therefore be beneficial (Jannin et al., 2008; Joyce et al., 2019).

To date, only a few studies have incorporated LBFs for poorly water-soluble drugs into 3D-printed solid dosage forms. A particular challenge is to ensure the rapid disintegration of the 3D-printed dosage form and subsequent release of the enabling drug formulation in the gastrointestinal tract. In a previous study, a drop-wise 3D-printing technique was used to produce an amorphous and self-emulsifying dosage form of celecoxib (Içten et al., 2017). In a proof of concept, Vithani and colleagues 3D-printed a solid LBF incorporating the poorly water-soluble drugs, fenofibrate or cinnarizine (Vithani et al., 2019). They combined lipid excipients and drug at high temperature to form a homogenous solution, then cooled it to form the solid dosage form. The solid LBF was loaded into a metal syringe, heated to 65 °C, and extruded into various tablet shapes. To date SSE has not been explored for its potential use to print LBFs into solid oral dosage forms. The current work therefore aimed to expand the use of 3D-printing technology for the production of solid lipid tablets. The well-studied compound fenofibrate was selected as model drug for which three different LBFs were transformed into printable emulsion gels. Solid lipid dosage forms were fabricated through SSE at room temperature. The study further aimed to produce rapidly disintegrating, uniform tablets for which the properties of the LBF, oil droplet size and lipid digestibility were retained during solidification.

2. Material and methods

2.1. Materials

Maisine CC (mixed long-chain glycerides) was kindly provided by Gattefossé (Lyon, France), Captex 355 EP/NF (medium-chain triglycerides) and Capmul MCM EP (mixed long-chain glycerides) by Abitec (Janesville, USA). Soybean oil (long-chain triglycerides), Kolliphor EL (polyethoxylated castor oil) and Tween 85, fenofibrate (≥99%), methyl cellulose (Methocel A4M), Nile red, porcine pancreatin extract (8 × USP specifications activity), 4-bromophenylboronic acid, trizma maleate, calcium chloride dihydrate, sodium hydroxide pellets, sodium acetate, acetic acid, silica gel, acetonitrile (≥99.9%) and 2-propanol (99.9%) were obtained from Merck (Darmstadt, Germany). Fasted-state simulated intestinal fluid (FaSSIF) powder was purchased from biorelevant.com (Croydon, UK) and croscarmellose sodium (Ac-Di-Sol) from FMC (Brussels, Belgium).

2.2. Lipid-based formulations and drug loading

Table 1 shows the LBF compositions included in this study: type II long-chain (II-LC), type IIIA long-chain (IIIA-LC), and medium-chain (IIIA-MC) (Table 1) (Williams et al., 2012). The LBFs were prepared as described previously (Alskär et al., 2016). In brief, excipients were preheated to 37 °C in an incubator (Termaks, Bergen, Norway), weighed directly into glass vials, vortexed, and placed on a shaker at 37 °C overnight under an inert N_2 atmosphere. The equilibrium solubility of fenofibrate in the LBFs was determined at room temperature, according to a previously described protocol (Alskär et al., 2016). An excess of fenofibrate was added to the LBF in a glass vial and left on a plate shaker at room temperature to equilibrate for 96 h before sampling. Prior to sampling, the vials were centrifuged (Eppendorf centrifuge 5810R, Hamburg, Germany) at, 2800g for 30 min at 22 °C. The supernatant (~30 mg) was transferred to a volumetric flask and diluted to 5 ml with 2-propanol. The drug concentration was determined at 287 nm in a 96-well UV-plate reader (Tecan, Safire, Zürich, Switzerland). Solubility measurements were performed in duplicate. Subsequently, the LBFs were loaded with 80% of the determined fenofibrate equilibrium solubility to reduce the risk of drug precipitation upon emulsification (Tables 1 and S1). The required amount of fenofibrate and LBF were weighed into glass vials, vortexed, and placed on a shaker at 37 °C until the drug dissolved completely.

2.3. Preparation of emulsions

Emulsions with an oil-to-water (O/W) ratio of 3:7 were prepared (Fig. 1a) by adding the required amount of drug loaded LBF (oil phase) to Milli-Q water (continuous phase; Merck, Darmstadt, Germany), followed by a two-step emulsification process (Fig. 1b). First, the O/W phases were ultrasonicated using a Vibra-Cell sonicator mounted with a 13 mm probe tip (Sonics, Newtown, CT, USA) operating at 20% amplitude, pulse 30 s on and 1 s off, for 5 min. This pre-emulsion was then processed 10 times at 1000 bar using a microfluidizer (LM20, Microfluidics, Westwood, MA, USA) with a diamond interaction chamber assembly (H10Z, 100 μm). The fenofibrate concentration in the emulsions was determined to check for any drug loss during processing. In brief, the emulsion was weighed (~100 mg) into 5 ml volumetric flasks and diluted with 2-propanol. Drug quantification was analyzed by HPLC (section 2.10). All measurements were performed in triplicate.

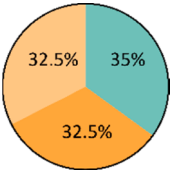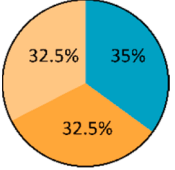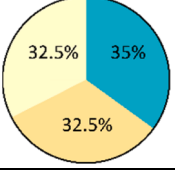### 2.4. Kinetic stability and droplet size characterization

The emulsion stability was evaluated visually and droplet size distribution was measured upon preparation as well as after 4 weeks of storage. For visual assessment of any phase separation during storage, drug loaded LBFs were stained with a small amount of Nile red prior to emulsification. Emulsions were aliquoted into glass vials, sealed under nitrogen gas, and stored in a desiccator with silica gel, at 25 °C for 4 weeks. The droplet size distribution was measured by dynamic light scattering (DLS; Litesizer 500, Anton Paar GmbH, Graz, Austria) at 25 °C. Prior to measurement, the emulsion was diluted 100-fold in Milli-Q water. A refractive index of 1.5 and an absorption coefficient of 0.005 were used. Measurements were conducted in triplicate.

2.5. Cryo scanning electron microscopy (cryo-SEM)

Emulsion morphology was imaged by a low-voltage field-emission cryogenic scanning electron microscope (cryo-SEM; Carl Zeiss Merlin, Oberkochen, Germany) fitted with a Quorum Technologies PP3000T cryo preparation system. Samples were vortexed briefly and high pressure frozen in the 100 μm side of a type A 6 mm carrier using an HPM100 (Leica microsystems, Wetzlar, Germany). The frozen samples were stored in liquid nitrogen prior to cryo-SEM imaging. Images were taken at −140 °C using an in-chamber secondary electron detector (ETD) at an
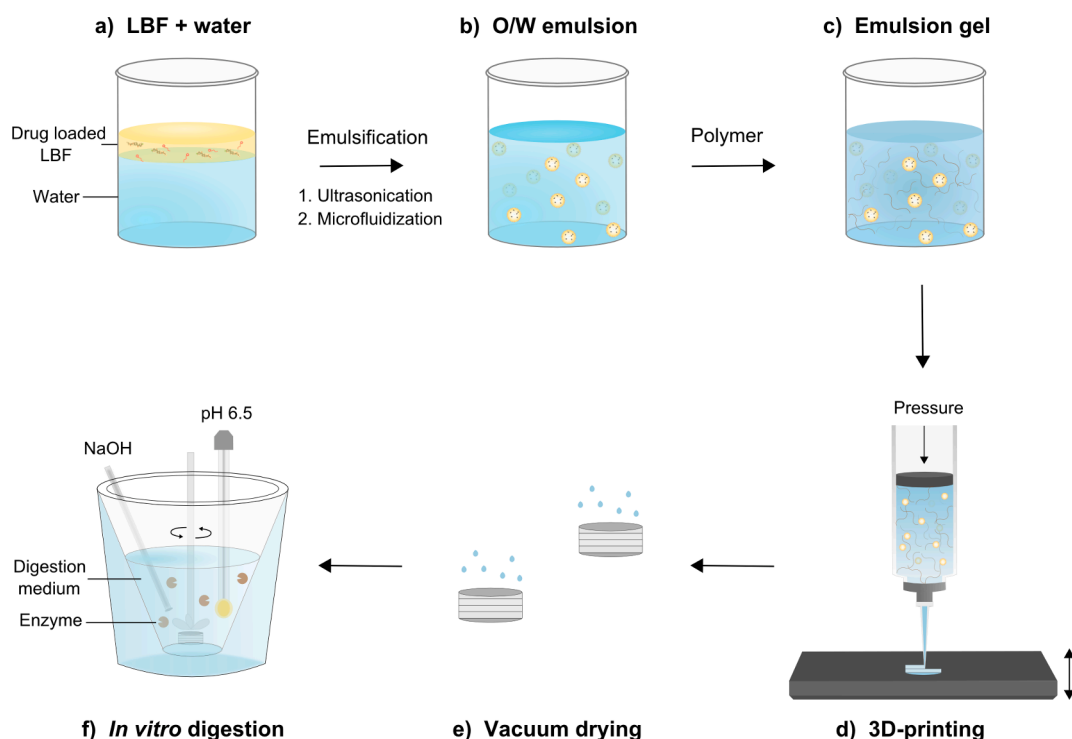
Table 1

Composition of lipid-based formulations (LBFs), printing parameters of emulsions gels, and physical characteristics of 3D-printed tablets. Values for weight and dimensions are expressed as mean; standard deviation (SD) is given in brackets, n = 3.

Formulation			Printing parameters		Physical parameters			
LBF Type*	Composition** (% w/w)	Drug load† (mg/g)	Pressure (kPa)	Speed (mm/sec)	Weight (mg)		Dimensions (mm)	
					Wet	Dry	Diameter	Thickness
II-LC	35% / 32.5% / 32.5%	45.0	55	2	243.4 (10.2)	110.1 (4.0)	8.5 (0.1)	2.5 (0.1)
IIIA-LC	35% / 32.5% / 32.5%	41.9	65	2	201.7 (8.9)	89.5 (2.2)	7.9 (0.1)	2.0 (0.2)
IIIA-MC	35% / 32.5% / 32.5%	53.2	55	2.5	269.1 (7.2)	122.0 (3.0)	8.5 (0.2)	2.1 (0.1)

* LBF II-LC: type II long-chain; IIIA-LC: type IIIA long-chain; IIIA-MC: type IIIA medium-chain.

** ■ Soybean oil; ■ Maisine CC; ■ Tween 85; ■ Kolliphor EL; ■ Captex 355 EP/NF; ■ Capmul MCM EP.

† Drug load corresponds to 80% of the equilibrium solubility of fenofibrate at room temperature.

Fig. 1. Schematics illustrating the preparation of printable emulsion gels, 3D-printing by semi-solid extrusion (SSE), and *in vitro* digestion of 3D-printed tablets. (a) Drug-loaded lipid-based formulation (LBF) was added to water, followed by (b) a two-step emulsification process. (c) Polymers were added to emulsified LBFs to generate printable emulsion gels. (d) The emulsion gels were 3D-printed by SSE into tablets, and (e) vacuum dried. (f) 3D-printed tablets were digested in an *in vitro* lipolysis set-up to quantify the release of free fatty acids (FAs).

accelerating voltage of 1 kV and probe current of 50 pA.

2.6. Preparation of emulsion gels

A 3D-printable hydrogel was prepared from the O/W emulsion by adding 12% (w/w) methyl cellulose and 5% (w/w) croscarmellose sodium (Fig. 1c). For this, the emulsion was weighed into a glass vial and preheated to 70 °C. Methyl cellulose, followed by croscarmellose sodium, was added gradually to the warm emulsion between cycles of vortexing and reheating. The final printable emulsion gel was placed at 4 °C overnight and vortexed periodically to dissolve the methyl cellulose.

2.7. Rheology

Rheological measurements of emulsion gels were performed on an Ares-G2 rheometer (TA instruments, New Castle, DE, USA). Flow curves with shear rates ranging from 1 to 100 s^{-1} were recorded with a stainless-steel, parallel-plate geometry (diameter = 25 mm, gap = 0.3035 mm) at 25 °C with five measurement points per decade and 30 sec equilibration between points.

2.8. 3D-printing

Emulsion gels were 3D-printed into tablets by SSE using a BIO X 3D-printer equipped with a pneumatic printhead (Fig. 1d; Cellink, Gothenburg, Sweden). A 3 ml cartridge was filled with emulsion gel and a printing nozzle with an inner diameter of 0.41 mm was mounted. The printing speed and pressure were adjusted for each of the emulsion gels to achieve appropriate printing. The pressure ranged from 55 to 65 kPa and the applied speed was 2–2.5 mm/sec (Table 1). The printing time of an individual tablet was 11–14 min. The 3D-model used for printing was a cylinder of 8 layers with a diameter of 10 mm and height of 3 mm. The infill density was 100% and printing was performed at room temperature. Tablets were printed directly onto a glass petri dish and subsequently dried in a vacuum oven at room temperature and 400 mbar overnight (Fig. 1e; Vacutherm, Thermo Fisher Scientific, Massachusetts, USA). To ensure sufficient drying, the tablets were further left to air dry for at least 24 h prior to characterization. Drying was considered complete when the deviation between the weight loss and theoretical amount of water in the tablets was less than 10%.

2.9. Characterization of 3D-printed tablets

2.9.1. Physical parameters
Diameter and thickness of the 3D-printed tablets were measured with a traceable digital caliper (VWR, Stockholm, Sweden). The weight of the tablets was measured after 3D-printing and after drying. All measurements were completed in triplicate.

2.9.2. In vitro disintegration of 3D-printed tablets
The *in vitro* disintegration test of 3D-printed tablets (n = 6) was performed using a basket-rack assembly with discs (Pharma Test PTZ-S, Hainburg, Germany). The test was performed as described in the European Pharmacopeia 9th edition. Briefly, a beaker was filled with approximately 650 ml distilled water and heated to 37.0 ± 0.5 °C. A single, 3D-printed tablet was placed in each of the 6 tubes in the basket and a cylindrical disc was added. The disintegration test was run for 15 min with a frequency rate of 30 cycles/min. The basket was lifted at the end of each test and the state of the tablets visually examined.

2.9.3. In vitro dispersion and digestion of 3D-printed tablets
The *in vitro* digestion of 3D-printed tablets (Fig. 1f) was performed according to a standardized lipolysis method (Williams et al., 2012). The setup consisted of a pH-stat (iUnitrode) coupled to a dosing unit (Metrohm 907 Titrando, Switzerland). A buffer (pH 6.5) comprising 2 mM

Tris–maleate, 1.4 mM CaCl$_2$·2H$_2$O and 150 mM NaCl with FaSSIF powder added (3.0 mM and 0.75 mM of sodium taurocholate and lecithin, respectively) was used as digestion medium. The pancreatic extract (7800 TBU/ml extract) was prepared by adding 6 ml buffer to 1.2 g porcine pancreatin. The mixture was vortexed thoroughly followed by centrifugation at 5 °C, 2144*g* for 15 min. The 3D-printed tablet was dispersed in 41.5 ml digestion medium for 30 min (at 450 rpm) in a temperature controlled glass vessel (37 °C). At the end of the dispersion phase, the pH was manually adjusted to 6.5 ± 0.05, and the droplet size of dispersed formulation was measured by DLS (Section 2.4). After the dispersion phase, 1 ml of sample was removed to determine the drug content in the 3D-printed tablet. The sample was diluted with 2-propanol to 5 ml in a volumetric flask and analyzed with HPLC (Section 2.10). To initiate digestion, 4.44 ml of enzyme extract was added to the lipolysis vessel. During *in vitro* digestion (60 min), the pH was maintained at 6.5 by automatic titration of 0.2 M (II-LC and IIIA-LC) or 0.6 M (IIIA-MC) NaOH solution. The extent of digestion was calculated by simplifying a previously described method (Williams et al., 2012):

$$\text{Extent digestion}(\%) = \frac{\text{Ionized FAs}}{\text{Theoretical FAs in LBF}} \times 100 \qquad (1)$$

where the quantity of ionized fatty acids (FAs) at pH 6.5 determined from the titrated amount of NaOH is related to the theoretical maximum amount of FAs that can be released from the lipid components in the LBFs upon digestion. The estimation was based on the assumption that one triglyceride molecule releases two FAs, while diglycerides and monoglycerides release one FA each. The *in vitro* dispersion and digestion experiments were performed in triplicate.

2.10. HPLC analysis

Prior to HPLC analysis, all samples were diluted in mobile phase followed by centrifugation at 22 °C, 21,000*g* for 15 min. Analysis was conducted using an HPLC (1290 Infinity, Agilent Technologies, Santa Clara, CA, USA) with a Zorbax Eclipse XDB-C18 column (4.6 × 100 mm) maintained at 40 °C. The mobile phase consisted of 80% acetonitrile and 20% (v/v) sodium acetate buffer (25 mM, pH 5.0). A flow rate of 1 ml/min was used resulting in a retention time of 3.36 min. The injection volume was 20 µl and UV absorbance measured at 287 nm. Quality control samples were used to assure accuracy of the analysis.

3. Results and discussion

3.1. Droplet size and kinetic stability of the emulsified LBFs

Stability of the three emulsified LBFs was studied by evaluating the droplet size distribution over time (Fig. 2a, Table S2). Droplet size of emulsified LBFs is influenced by the amount and type of excipients in the formulations and chain length of the lipids (Williams et al., 2012). Both LBF type IIIA emulsions containing the water-soluble surfactant Kolliphor EL (HLB 12–14) had a smaller droplet size than the LBF type II containing Tween 85 (HLB 11). The hydrodynamic diameter of emulsified LBFs ranged from 31 to 103 nm and followed the rank-order II-LC > IIIA-LC > IIIA-MC, in agreement with previous LBF measurements (Williams et al., 2012). The oil droplet size was further verified by cryo-SEM images of the emulsified LBFs (Fig. S1). The droplet size for all three emulsions following storage was similar to the initial measurements, indicating that the emulsions were stable at room temperature for up to one month without phase separation. In addition, all three emulsions showed a continued narrow size distribution, polydispersity index < 0.1 after storage (Table S2). Storage stability was further confirmed by Nile red staining of the oil phase (Fig. S2). Hence, storage stability essential for dose homogeneity in the final 3D-printed tablet was confirmed.
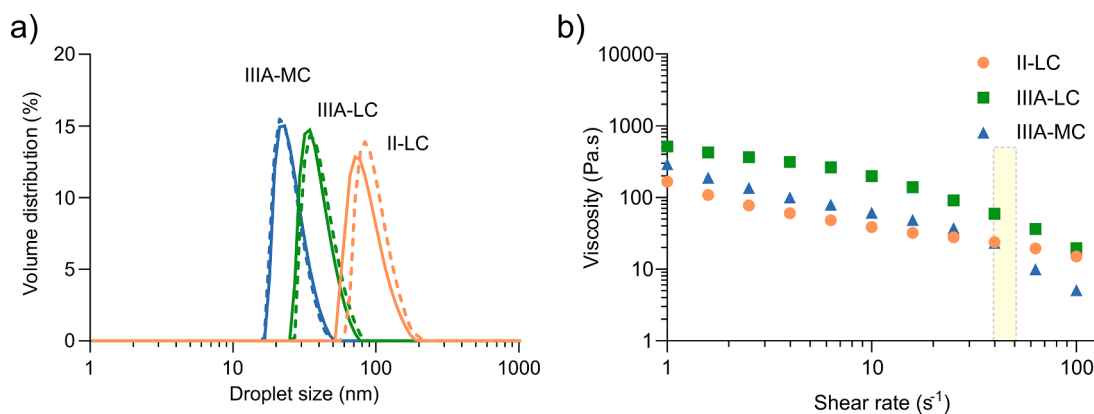
Fig. 2. Storage stability of emulsions and rheology of printable emulsion gels. (a) Droplet size distribution for LBF type II-LC, IIIA-LC, and IIIA-MC emulsions upon preparation (solid lines) and after 4 weeks' storage at 25 °C (dashed lines). Values are expressed as the mean, (n = 3). (b) Viscosity as a function of shear rate for emulsion gels of LBF type II-LC (circles), IIIA-LC (squares), and IIIA-MC (triangles). Yellow area visualizes the calculated range in maximum shear rate during 3D-printing (Eq. (2)).

3.2. Rheological behavior of printable emulsion gels

Appropriate rheological properties of emulsion gels are critical for successful 3D-printing of solid dosage forms (Jungst et al., 2016). Here, methyl cellulose was used as a viscosity modifier to achieve sufficiently high viscosity and the desired non-Newtonian, shear-thinning behavior of emulsion gels for 3D-printing (Dai et al., 2019). Emulsion gels experience a maximum shear rate at the walls as they flow through the nozzle tip during 3D-printing. The maximum shear rate $\dot{\gamma}_{max}$ can be estimated from (M'Barki et al., 2017):

$$\dot{\gamma}_{max} = \frac{\left(4 \times \dot{Q}\right)}{\pi \times r^3} = \frac{4S}{r} \tag{2}$$

where $\dot{Q}$ is the volumetric flow rate, S is the printing speed, and r is the radius of the nozzle. With the printing speeds here (Table 1), this corresponds to maximum shear rates in the range 40–50 s^{-1}. The apparent viscosity profiles as a function of shear rate of the emulsion gels are shown in Fig. 2b. The apparent viscosity decreased with increasing shear rate for all emulsion gels, characteristic for their shear-thinning behavior. This rheological property of methyl cellulose gels is well known (Polamaplly et al., 2019). Hydrogen bonds between cellulose chains break during extrusion, allowing the chains to align with the flow direction, thereby reducing viscosity (Dai et al., 2019). LBF type IIIA-LC displayed the highest apparent viscosity at 40 s^{-1} of the three LBFs and hence, required the highest pressure for printing (65 kPa for IIIA-LC and 55 kPa for the other two; Table 1). The flow curves obtained for the LBF type II-LC and IIIA-MC emulsion gels were fitted using the Herschel-Bulkley formula:

$$\sigma = \sigma_y^{dyn} + K\dot{\gamma}^n \tag{3}$$

where σ is the stress (Pa), σ_y^{dyn} is the dynamic yield stress (Pa), K is a model factor referred to as the consistency index (Pa·s^n), $\dot{\gamma}$ is the shear rate (s^{-1}) and n is the flow index (M'Barki et al., 2017; Polamaplly et al., 2019). For LBF type IIIA-LC power law was applied:

$$\sigma = K\dot{\gamma}^n \tag{4}$$

A flow index $n < 1$ was obtained for all emulsion gels (Table S4), thus indicating shear-thinning behavior. LBF type II-LC and IIIA-MC displayed rather similar flow index values, suggesting that the LBF composition had minimal influence on the rheological properties.
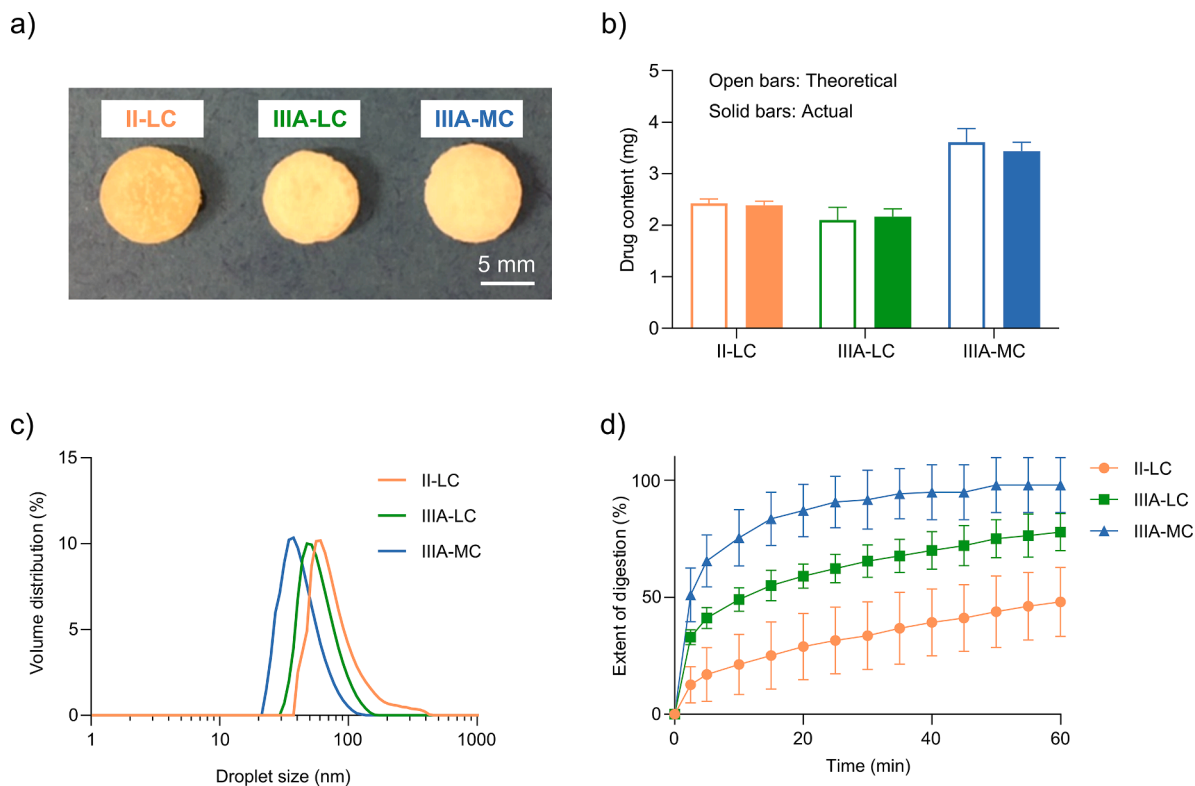
3.3. 3D-printing of tablets

The LBF emulsion gels were successfully 3D-printed into solid dosage forms using SSE at room temperature (Fig. 3a). The 3D-printed tablets appeared white to yellow depending on the formulation. All three emulsion gels were 3D-printed according to a predefined geometry with a diameter of 10 mm and thickness of 3 mm. To obtain well-defined printed tablets, printing parameters including pressure and speed were adjusted for each emulsion gel. As a result, the final weight, size, and dose of the tablets varied for the three printable emulsion gels (Table 1). The weight of the tablets was determined directly after 3D-printing (wet weight) and after drying (dry weight). Overall, a weight loss of 55% after drying was consistent for all formulations, correlating with the water content in the emulsion gel. Although the physical parameters of the 3D-printed tablets varied for the different emulsion gels, each formulation demonstrated good mass uniformity of printed tablets with a weight deviation <5%. After drying, 3D-printed tablets showed appropriate mechanical properties for easy handling, without risk of breaking or deformation. However, a tablet hardness test could not be performed of 3D-printed tablets after drying, as they were softer than compressed ones, in agreement with previous findings (Khaled et al., 2014). This was as expected, because compression forces in traditional tablet manufacturing are not a part of the 3D-printing process. In the case of SSE, tablet hardness can be controlled by including a binder in the formulation. After drying, the tablets shrank, resulting in a final diameter of 7.9–8.5 mm and thickness of 2–2.5 mm. An extensive drying step is common post-printing with SSE to ensure sufficient solidification. Previously, vacuum drying, at 40 °C for 24 h has been used to ensure complete drying of printed tablets (Khaled et al., 2015a). Here, vacuum drying at room temperature was used to avoid melting the lipid components in the 3D-printed tablets. In summary, the 3D-printed tablets showed highly reproducible mass and dimensions, and retained their physical shape after drying.

3.4. In vitro disintegration

The disintegration time of 3D-printed tablets was determined in aqueous solution, in conformity with pharmacopeia specifications. The 3D-printed tablets fulfilled the specification for uncoated tablets according to pharmacopeia and disintegrated completely within 15 min. The addition of 5% (w/w) croscarmellose sodium as a disintegrant provided rapid disintegration for these formulations, well in line with demands for immediate release tablets. In contrast FDM printing, which uses a high percentage of polymer, often gives slow disintegration and drug release, resulting in extended drug release patterns (Goyanes et al., 2014; Skowyra et al., 2015). A previous attempt to modify drug release from FDM printed tablets includes changing the infill density; however, this also affects the drug load in the 3D-printed tablet, something that

Fig. 3. *In vitro* characterization of 3D-printed tablets consisting of emulsified LBF type II-LC, IIIA-LC, and IIIA-MC. (a) Images of the 3D-printed tablets. (b) Amount of fenofibrate in 3D-printed tablets. Open bars represent the theoretical drug content and solid bars the actual one. Values are expressed as the mean ± SD, n = 3. (c) Droplet size distribution after 30 min dispersion of 3D-printed tablets in digestion medium (37 °C). Values are expressed as the mean, n = 3. (d) The estimated extent (%) of *in vitro* digestion during 60 min (37 °C). The estimation was based on the quantity of ionized FAs at pH 6.5 compared to the theoretical maximum amount of FAs released from the lipid components in the LBFs (Eq. (1)). Values are expressed as the mean ± SD, n = 3.

already limits the use of this 3D-printing technique (Goyanes et al., 2015, 2014). The application of an extrusion based 3D-printing technique in this study allowed production of tablets with 100% infill density with a rapid disintegration time.

3.5. Drug content in 3D-printed tablets

The LBFs studied here were loaded with fenofibrate, a poorly-water soluble model drug, at 80% of its equilibrium solubility in each of the formulations. Hence, the dose in the printed tablets varied as we explored the printable dose of fenofibrate using these LBFs. Dispersion of LBFs can result in a rapid loss of their solubilization capacity, in particular for the more hydrophilic LBF types IIIB and IV (Mohsin et al., 2009; Williams et al., 2013). Fenofibrate was fully recovered in the emulsified LBFs, thereby confirming that no drug precipitation had occurred during emulsification (Fig. S3). The drug content in the final 3D-printed tablets correlated well with the theoretical drug loading (Fig. 3b). This indicates that the dose in 3D-printed tablets was completely released within 30 min of dispersion. The average drug load of 2.5% (w/w) was lower than in a previous study with self-microemulsifying drug delivery system that had 7% (w/w) fenofibrate 3D-printed into tablets with different geometrical shapes (Vithani et al., 2019). However, the approach presented by Vithani and colleagues required heating during both formulation and extrusion. Crystalline drug particles appeared within the 3D-printed solid self-microemulsifying drug delivery system, which might have been a result of recrystallization upon cooling. In this study, the 3D-printing was carried out at room temperature and hence, the methodology is highly attractive for thermolabile drug compounds and formulations.

The maximum amount of drug included in the 3D-printed tablet will be highly dependent on the drug itself, the LBF components and their respective weight fractions. LBF type IIIA-MC, having the highest loading capacity among the included LBFs here, resulted in the highest drug load (2.7% w/w) of 3D-printed tablets. The higher loading capacity is consistent with previous work showing a general trend of higher drug solubility in MC than LC triglycerides (Alskär et al., 2016). The more lipid-rich LBFs usually have poorer loading capacity. However, they are unlikely to lose that capacity upon dispersion, which can happen in LBFs with higher fractions of surfactant and cosolvent. This loss in solvation capacity risks drug precipitation (Mohsin et al., 2009; Williams et al., 2013). Overall, the drug load in 3D-printed tablets is limited by the loading capacity of the LBFs. Fenofibrate was in this study selected as a model compound for lipophilic, poorly water-soluble drugs, and a therapeutically active product for the compound as such was not our aim. The relatively low drug load in the explored formulations limits relevant oral doses of fenofibrate to be printed. However, the approach presented here is expected to be universal, mainly suitable for drug delivery of potent lipophilic drug compounds, which can be administered at low dose. Moreover, the good uniformity in drug content suggests 3D-printing of emulsion gels into tablets to be a promising method for manufacturing tablets with a high dose accuracy.

3.6. In vitro dispersion and digestion

The size of oil droplets upon dispersion influences the surface area available for enzyme binding and digestion (Nielsen et al., 2008; Patton and Carey, 1979). In order to evaluate the potential to reconstitute the droplet size of emulsified LBFs after tablet disintegration, the droplet size of dispersed 3D-printed tablets was measured (Fig. 3c). The droplet size rank-order (II-LC > IIIA-LC > IIIA-MC) was the same after dispersion of 3D-printed tablets as for the starting emulsions (Fig. 2a). However, the redispersed size distribution was broader and slightly larger

than the droplet size of pure emulsified LBFs (Table S3). This can be attributed to the presence of other excipients (croscarmellose sodium and methyl cellulose) in the printed tablets (size distribution of dispersed polymeric excipients: Fig. S4).

The lipid digestion of 3D-printed tablets was studied after dispersion. Fig. 3d shows the extent of lipid digestion of the printed emulsion gels. After 60 min it was almost complete for LBF type IIIA-MC (98%), whereas type IIIA-LC and type II-LC were digested to 78% and 48%, respectively. This corresponds well with the extent of digestion of these LBFs in a previous study (Williams et al., 2012). In our study, the calculation to estimate the extent of digestion was simplified in two main aspects. First, a back-titration step was omitted. This means that unionized fatty acids at pH 6.5 were not taken into account. Previous work shows that the quantity of unionized FAs at pH 6.5 increases with LBF lipophilicity and is higher for LC than MC lipid formulations (Williams et al., 2012). Second, digestion of surfactant (Tween 85 or Kolliphor EL) in the LBFs was not included in the theoretical quantity of FAs in the LBFs (Eq. (1).). The LBFs comprised equal quantities of surfactant, but differed in surfactant type. On the basis of a previous study, the surfactants used here are probably digested to some extent (Cuiné et al., 2008). Overall, the results from the *in vitro* digestion of 3D-printed tablets showed that the LBF successfully redispersed from the tablets. The reconstituted LBF emulsions had fine oil-droplet sizes and their digestion profiles were in line with traditional liquid LBFs. In summary, this demonstrates that the beneficial properties of LBFs are retained in 3D-printed tablets based on emulsion gels.

4. Conclusion

Solid lipid tablets with fenofibrate as a model poorly water-soluble drug were successfully produced by SSE of emulsion gels at room temperature. Three different types of LBFs were emulsified and transformed into printable emulsion gels with suitable rheological properties for 3D-printing by addition of methyl cellulose as viscosity enhancer. The 3D-printed tablets had appropriate mechanical properties for handling, and were well-defined in size with high mass uniformity and dose accuracy. The printed tablets disintegrated rapidly (<15 min), in-line with the demands for immediate release tablets. The oil droplet size of emulsified LBFs was reconstituted and the 3D-printed tablets demonstrated a lipid digestion in agreement with traditional liquid LBFs. In summary, our study demonstrates the use of SSE to produce solid lipid tablets, thereby combining the advantages of LBFs as an established formulation strategy for poorly water-soluble drugs with a 3D-printing technology for solidification and flexible production. The methodology opens up for possibilities of 3D-printing in hospital pharmacies of highly potent, poorly water-soluble drugs, for which flexible dose adjustments may be needed for patient population groups such as children and elderly.

CRediT authorship contribution statement

Jenny Johannesson: Conceptualization, Methodology, Investigation, Writing - original draft, Visualization. **Jamal Khan:** Conceptualization, Methodology, Investigation, Writing - original draft, Visualization. **Madlen Hubert:** Conceptualization, Investigation, Writing - original draft. **Alexandra Teleki:** Conceptualization, Writing - original draft, Supervision, Funding acquisition. **Christel A.S. Bergström:** Conceptualization, Writing - review & editing, Supervision, Funding acquisition.

Declaration of Competing Interest

The authors declare that they have no known competing financial interests or personal relationships that could have appeared to influence the work reported in this paper.

Appendix A. Supplementary material

Supplementary data to this article can be found online at https://doi.org/10.1016/j.ijpharm.2021.120304.

References

Alskär, L.C., Porter, C.J.H., Bergström, C.A.S., 2016. Tools for early prediction of drug loading in lipid-based formulations. Mol. Pharm. 13, 251–261. https://doi.org/10.1021/acs.molpharmaceut.5b00704.

Awad, A., Trenfield, S.J., Goyanes, A., Gaisford, S., Basit, A.W., 2018. Reshaping drug development using 3D printing. Drug Discov. Today 23, 1547–1555. https://doi.org/10.1016/j.drudis.2018.05.025.

Bergström, C.A.S., Charman, W.N., Porter, C.J.H., 2016. Computational prediction of formulation strategies for beyond-rule-of-5 compounds. Understanding the challenges of beyond-rule-of-5 compounds. Adv. Drug Deliv. Rev. 101, 6–21. https://doi.org/10.1016/j.addr.2016.02.005.

Bjerknes, K., Bøyum, S., Kristensen, S., Brustugun, J., Wang, S., 2017. Manipulating tablets and capsules given to hospitalised children in Norway is common practice. Acta Paediatr. 106, 503–508. https://doi.org/10.1111/apa.13700.

Boyd, B.J., Bergström, C.A.S., Vinarov, Z., Kuentz, M., Brouwers, J., Augustijns, P., Brandl, M., Bernkop-Schnürch, A., Shrestha, N., Préat, V., Müllertz, A., Bauer-Brandl, A., Jannin, V., 2019. Successful oral delivery of poorly water-soluble drugs both depends on the intraluminal behavior of drugs and of appropriate advanced drug delivery systems. Eur. J. Pharm. Sci. 137, 104967 https://doi.org/10.1016/j.ejps.2019.104967.

Cuiné, J.F., McEvoy, C.L., Charman, W.N., Pouton, C.W., Edwards, G.A., Benameur, H., Porter, C.J.H., 2008. Evaluation of the impact of surfactant digestion on the bioavailability of danazol after oral administration of lipidic self-emulsifying formulations to dogs. J. Pharm. Sci. 97, 995–1012. https://doi.org/10.1002/jps.21246.

Dai, L., Cheng, T., Duan, C., Zhao, W., Zhang, W., Zou, X., Aspler, J., Ni, Y., 2019. 3D printing using plant-derived cellulose and its derivatives: A review. Carbohydr. Polym. 203, 71–86. https://doi.org/10.1016/j.carbpol.2018.09.027.

El Aita, I., Rahman, J., Breitkreutz, J., Quodbach, J., 2020. 3D-Printing with precise layer-wise dose adjustments for paediatric use via pressure-assisted microsyringe printing. Eur. J. Pharm. Biopharm. 157, 59–65. https://doi.org/10.1016/j.ejpb.2020.09.012.

Firth, J., Basit, A.W., Gaisford, S., 2018. The role of semi-solid extrusion printing in clinical practice. In: Basit, A.W., Gaisford, S. (Eds.), 3D Printing of Pharmaceuticals, AAPS Advances in the Pharmaceutical Sciences Series. Springer International Publishing, Cham, pp. 133–151. https://doi.org/10.1007/978-3-319-90755-0_7.

Goyanes, A., Buanz, A.B.M., Basit, A.W., Gaisford, S., 2014. Fused-filament 3D printing (3DP) for fabrication of tablets. Int. J. Pharm. 476, 88–92. https://doi.org/10.1016/j.ijpharm.2014.09.044.

Goyanes, A., Buanz, A.B.M., Hatton, G.B., Gaisford, S., Basit, A.W., 2015. 3D printing of modified-release aminosalicylate (4-ASA and 5-ASA) tablets. Eur. J. Pharm. Biopharm. 89, 157–162. https://doi.org/10.1016/j.ejpb.2014.12.003.

Goyanes, A., Madla, C.M., Umerji, A., Duran Piñeiro, G., Giraldez Montero, J.M., Lamas Diaz, M.J., Gonzalez Barcia, M., Taherali, F., Sánchez-Pintos, P., Couce, M.-L., Gaisford, S., Basit, A.W., 2019. Automated therapy preparation of isoleucine formulations using 3D printing for the treatment of MSUD: First single-centre, prospective, crossover study in patients. Int. J. Pharm. 567, 118497 https://doi.org/10.1016/j.ijpharm.2019.118497.

Içten, E., Purohit, H.S., Wallace, C., Giridhar, A., Taylor, L.S., Nagy, Z.K., Reklaitis, G.V., 2017. Dropwise additive manufacturing of pharmaceutical products for amorphous and self emulsifying drug delivery systems. Int. J. Pharm. 524, 424–432. https://doi.org/10.1016/j.ijpharm.2017.04.003.

Jannin, V., Musakhanian, J., Marchaud, D., 2008. Approaches for the development of solid and semi-solid lipid-based formulations. Lipid-based systems for the enhanced delivery of poorly water soluble drugs. Adv. Drug Deliv. Rev. 60, 734–746. https://doi.org/10.1016/j.addr.2007.09.006.

Joyce, P., Dening, T.J., Meola, T.R., Schultz, H.B., Holm, R., Thomas, N., Prestidge, C.A., 2019. Solidification to improve the biopharmaceutical performance of SEDDS: Opportunities and challenges. Self-emulsifying drug delivery systems (SEDDS). Adv. Drug Deliv. Rev. 142, 102–117. https://doi.org/10.1016/j.addr.2018.11.006.

Jungst, T., Smolan, W., Schacht, K., Scheibel, T., Groll, J., 2016. Strategies and molecular design criteria for 3D printable hydrogels. Chem. Rev. 116, 1496–1539. https://doi.org/10.1021/acs.chemrev.5b00303.

Khaled, S.A., Alexander, M.R., Wildman, R.D., Wallace, M.J., Sharpe, S., Yoo, J., Roberts, C.J., 2018. 3D extrusion printing of high drug loading immediate release paracetamol tablets. Int. J. Pharm. 538, 223–230. https://doi.org/10.1016/j.ijpharm.2018.01.024.

Khaled, S.A., Burley, J.C., Alexander, M.R., Roberts, C.J., 2014. Desktop 3D printing of controlled release pharmaceutical bilayer tablets. Int. J. Pharm. 461, 105–111. https://doi.org/10.1016/j.ijpharm.2013.11.021.

Khaled, S.A., Burley, J.C., Alexander, M.R., Yang, J., Roberts, C.J., 2015a. 3D printing of tablets containing multiple drugs with defined release profiles. The potential for 2D and 3D printing to pharmaceutical development. Int. J. Pharm. 494, 643–650. https://doi.org/10.1016/j.ijpharm.2015.07.067.

Khaled, S.A., Burley, J.C., Alexander, M.R., Yang, J., Roberts, C.J., 2015b. 3D printing of five-in-one dose combination polypill with defined immediate and sustained release profiles. J. Controll. Release 217, 308–314. https://doi.org/10.1016/j.jconrel.2015.09.028.

M'Barki, A., Bocquet, L., Stevenson, A., 2017. Linking rheology and printability for dense and strong ceramics by direct ink writing. Sci. Rep. 7, 1–10. https://doi.org/10.1038/s41598-017-06115-0.

Mohsin, K., Long, M.A., Pouton, C.W., 2009. Design of lipid-based formulations for oral administration of poorly water-soluble drugs: precipitation of drug after dispersion of formulations in aqueous solution. J. Pharm. Sci. 98, 3582–3595. https://doi.org/10.1002/jps.21659.

Nielsen, F.S., Petersen, K.B., Müllertz, A., 2008. Bioavailability of probucol from lipid and surfactant based formulations in minipigs: Influence of droplet size and dietary state. Eur. J. Pharm. Biopharm. 69, 553–562. https://doi.org/10.1016/j.ejpb.2007.12.020.

Norman, J., Madurawe, R.D., Moore, C.M.V., Khan, M.A., Khairuzzaman, A., 2017. A new chapter in pharmaceutical manufacturing: 3D-printed drug products. Editor's Collection 2016. Adv. Drug Deliv. Rev. 108, 39–50. https://doi.org/10.1016/j.addr.2016.03.001.

Öblom, H., Sjöholm, E., Rautamo, M., Sandler, N., 2019. Towards printed pediatric medicines in hospital pharmacies: Comparison of 2D and 3D-printed orodispersible warfarin films with conventional oral powders in unit dose sachets. Pharmaceutics 11, 334. https://doi.org/10.3390/pharmaceutics11070334.

Okwuosa, T.C., Pereira, B.C., Arafat, B., Cieszynska, M., Isreb, A., Alhnan, M.A., 2017. Fabricating a shell-core delayed release tablet using dual FDM 3D printing for patient-centred therapy. Pharm. Res. 34, 427–437. https://doi.org/10.1007/s11095-016-2073-3.

Patton, J.S., Carey, M.C., 1979. Watching fat digestion. Science 204, 145–148. https://doi.org/10.1126/science.432636.

Polamaplly, P., Cheng, Y., Shi, X., Manikandan, K., Zhang, X., Kremer, G.E., Qin, H., 2019. 3D printing and characterization of hydroxypropyl methylcellulose and methylcellulose for biodegradable support structures. Polymer 173, 119–126. https://doi.org/10.1016/j.polymer.2019.04.013.

Pouton, C.W., 1997. Formulation of self-emulsifying drug delivery systems. Adv. Drug Deliv. Rev. 25, 47–58. https://doi.org/10.1016/S0169-409X(96)00490-5.

Rani, S., Rana, R., Saraogi, G.K., Kumar, V., Gupta, U., 2019. Self-emulsifying oral lipid drug delivery systems: advances and challenges. AAPS PharmSciTech 20, 129. https://doi.org/10.1208/s12249-019-1335-x.

Skowyra, J., Pietrzak, K., Alhnan, M.A., 2015. Fabrication of extended-release patient-tailored prednisolone tablets via fused deposition modelling (FDM) 3D printing. Eur. J. Pharm. Sci. 68, 11–17. https://doi.org/10.1016/j.ejps.2014.11.009.

Trenfield, S.J., Awad, A., Goyanes, A., Gaisford, S., Basit, A.W., 2018. 3D printing pharmaceuticals: Drug development to frontline care. Trends Pharmacol. Sci. 39, 440–451. https://doi.org/10.1016/j.tips.2018.02.006.

Vithani, K., Goyanes, A., Jannin, V., Basit, A.W., Gaisford, S., Boyd, B.J., 2019. A proof of concept for 3D printing of solid lipid-based formulations of poorly water-soluble drugs to control formulation dispersion kinetics. Pharm. Res. 36, 102. https://doi.org/10.1007/s11095-019-2639-y.

van der Vossen, A.C., Al-Hassany, L., Buljac, S., Brugma, J.-D., Vulto, A.G., Hanff, L.M., 2019. Manipulation of oral medication for children by parents and nurses occurs frequently and is often not supported by instructions. Acta Paediatr. 108, 1475–1481. https://doi.org/10.1111/apa.14718.

Williams, H.D., Sassene, P., Kleberg, K., Bakala-N'Goma, J.-C., Calderone, M., Jannin, V., Igonin, A., Partheil, A., Marchaud, D., Jule, E., Vertommen, J., Maio, M., Blundell, R., Benameur, H., Carrière, F., Müllertz, A., Porter, C.J.H., Pouton, C.W., 2012. Toward the establishment of standardized in vitro tests for lipid-based formulations, part 1: method parameterization and comparison of in vitro digestion profiles across a range of representative formulations. J. Pharm. Sci. 101, 3360–3380. https://doi.org/10.1002/jps.23205.

Williams, H.D., Sassene, P., Kleberg, K., Calderone, M., Igonin, A., Jule, E., Vertommen, J., Blundell, R., Benameur, H., Müllertz, A., Pouton, C.W., Porter, C.J.H., On behalf of the LFCS Consortium, 2013. Toward the establishment of standardized in vitro tests for lipid-based formulations, Part 3: Understanding supersaturation versus precipitation potential during the in vitro digestion of Type I, II, IIIA, IIIB and IV lipid-based formulations. Pharm. Res. 30, 3059–3076. https://doi.org/10.1007/s11095-013-1038-z.